Single-Inductor, Dual-Input CCM Boost Converter for Multi-Junction PV Energy Harvesting

by

Qirong Peng

A Thesis Presented in Partial Fulfillment
of the Requirements for the Degree
Master of Science

Approved May 2017 by the
Graduate Supervisory Committee:

Sayfe Kiaei, Chair
Bertan Bakkaloglu
Umit Ogras

ARIZONA STATE UNIVERSITY

August 2017

ABSTRACT

This thesis presents a power harvesting system combining energy from sub-cells of multi-junction photovoltaic (MJ-PV) cells. A dual-input, inductor time-sharing boost converter in continuous conduction mode (CCM) is proposed. A hysteresis inductor current regulation in designed to reduce cross regulation caused by inductor-sharing in CCM. A modified hill climbing algorithm is implemented to achieve maximum power point tracking (MPPT). A dual-path architecture is implemented to provide a regulated 1.8V output. A proposed lossless current sensor monitors transient inductor current and a time-based power monitor is proposed to monitor PV power. The PV input provides power of 65mW. Measured results show that the peak efficiency achieved is around 85%. The power switches and control circuits are implemented in standard 0.18um CMOS process.

ACKNOWLEDGMENTS

I want to express my sincere gratitude to my thesis advisor and committee chair, Dr. Sayfe Kiaei, for advising this challenging project.

I want to thank Dr. Bertan Bakkaloglu and Dr. Umit Ogras for being my committee Members.

Also, I want thank Debashis Mandal, Yu Geng, Shrikant Singh, Chai Yong Lim, Parisa Mahmoudidaryan and Amir Ayati for their help and support on this project.

TABLE OF CONTENTS

Page

CHAPTER Page

LIST OF TABLES

Table Page

LIST OF FIGUIRES

Figure Page

Figure Page

Chapter 1

INTRODUCTION

1.1 Multi-Junction PV Cells

With increasing global demand for energy, solar energy industry is growing rapidly. Single junction PV (SJ-PV) cells utilize a fraction of the solar spectrum depending on the bandgap of the PV material. An ideal SJ-PV cell achieves maximum efficiency of 31% [1], while MJ-PV cells are evolved to extract energy from a wider solar spectrum and ideally achieves 72% efficiency [1]. The state-of-the-art PV cells show that double-junction cells, triple-junction cells, and now quadruple-junction cells are the driving force to increase efficiency of PV cells. MJ-PV cells with efficiencies over 40% are now common [2]-[6]. Because of their high efficiency potentials, MJ-PV cells are widely used in space and terrestrial applications, and are being investigated by both academic institutions and industries.

Power-voltage characteristic of a SJ-PV cell exhibits a unique operating point where the PV generated power is maximized (maximum power point, MPP). The MPP changes with continuously changing solar irradiation and ambient temperature conditions. Many MPP tracking (MPPT) methods are developed to operate the PV at the MPP [7]. The sub-cell characteristics of a MJ-PV cell are different from each other as shown in Fig. 1.1. If all these sub-cells with different bandgap energies are connected in series, current mismatch among sub-cells results in very low short circuit current and reduces the efficiency; while connecting all sub-cells in parallel causes voltage mismatch and the

system produces very low output voltage for any power conversion. Individual sub-cell in MJ-PV cell has different MPP and each sub-cell needs separate MPPT circuit for efficient power conversion efficiency. Therefore, sub-cell-level MPPT is required for MJ-PV cells.

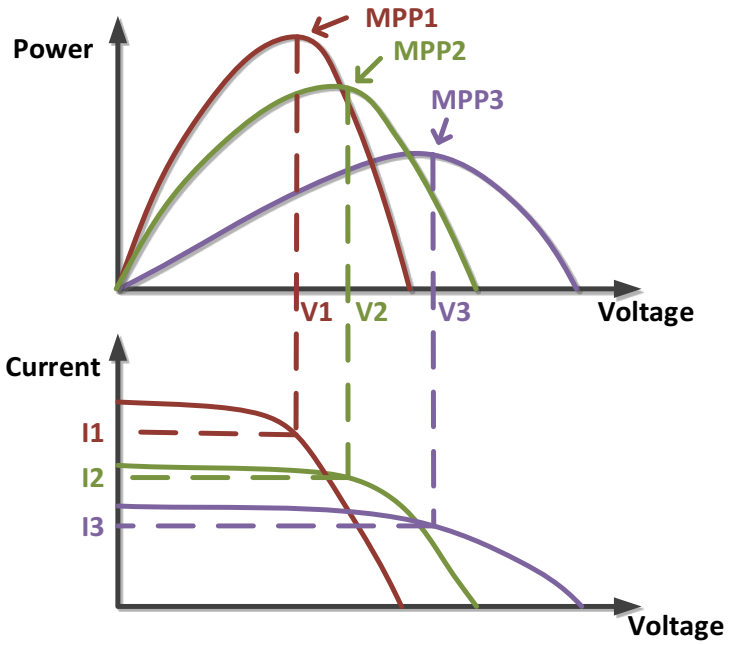

Fig. 1.1 P-V and I-V Characteristics of a Multi-Junction PV Cell

A DC-DC power converter with MPP tracking algorithm is the most used technique to extract maximum power from a SJ-PV cell, and the MPP operation of the PV cell is achieved by matching the input impedance of DC-DC converter to the output impedance of the PV cell at the MPP. One of the most common MPPT techniques is hill climbing [7] - [10]. Compared to other MPPT techniques, such as, incremental conductance [11]-[12] and ripple correlation control (RCC) [13], hill climbing has the simplest circuit implementation. To obtain a stable regulated output voltage, another DC-DC converter as second stage is usually used. However, cascading two boost converters increases

component count and decreases overall system power efficiency, a dual-paths structure at the output is proposed in [14] to achieve both MPPT and output regulation using a single DC-DC converter.

1.2 Prior Work Limitations

Although there is an extensive research on MJ-PV cell efficiency improvement, limited research materials are available on cost-effective, efficient power management circuits for maximum power generation from MJ-PV cells. The most straightforward technique for MPP operation of MJ-PV cells is to use a DC-DC converter with MPPT algorithm for each sub-cell. In [15], a sub-cell interconnection system is proposed and implemented on PCB (printed circuit board) level using off-the-shelf components. To increase current and voltage levels, strings are formed by connecting sub-cells made from the same material in series and parallel, and string-level MPPT is performed. The outputs of four converters are connected to a DC bus. It achieves peak efficiency of 90% at around 40W. However, for a four-layer MJ-PV cell, four strings are formed and four DC-DC converters are used to achieve MPPT, which increases energy harvesting cost.

To decrease number of converters and expensive components (such as off-chip inductors), multi-input energy harvesting systems with inductor time-sharing DC-DC converter has been proposed [14], [16] and [17]. The main challenge of inductor time-sharing is cross regulation of the input. There are two ways in existing work to suppress cross-regulation. On the one hand, [16] uses diode between input PV cells and boost converter to reduce ringing at the converter input node. [14] and [17] operates the converter

in discontinuous conduction mode (DCM) and pseudo continuous conduction mode (PCCM) respectively to ensure that the inductor current is either zero or at a constant value when switching between sub-cells. However, both DCM and PCCM causes large inductor current. Therefore neither of these are power-efficient solutions for sub-cell level MJ-PV cell power management.

1.3 Highlight of this Work

This thesis proposes a single inductor, dual-input boost converter with MPPT at each input, operating in CCM at power level of a few hundred milli-watts for MJ-PV applications. To reduce the cross-regulation among PV sub-cells, a constant inductor current-based controller is proposed. A hysteresis current loop is used to control inductor current. A modified hill climbing algorithm is implemented to achieve MPPT. A dual-path structure with hysteresis control is used to regulate the output voltage. The proposed converter has two PV inputs and generates two boosted voltages V_{OUT} and V_{STORE}. V_{OUT} is used as a supply voltage for internal application circuits, and extra power that load (application circuit) does not require will be stored in a battery storage. Fig. 1.2 shows a top-level block diagram of an energy harvesting system for MJ-PV cells with proposed inductor time-sharing DC-DC boost converter.

1.4 Thesis Organization

The rest of the thesis is organized as follows. Chapter 2 discusses prior works on PV energy harvesting. Section 2.1-2.3 focuses on the characteristic of PV cells and basic

architecture and techniques for SJ-PV energy harvesting. Section 2.4 presents existing work on multi-input, inductor time-sharing boost converters for PV cells. Chapter 3 explains the challenges of inductor time-sharing in CCM operation and highlights system architecture. It explains the converter control scheme, MPPT algorithm and implementation, and dual-path output regulation. Chapter 4 focuses on circuit implementation of inductor current sensor and PV power monitor. Section 5 presents measurement results, and finally it concluded in chapter 6.

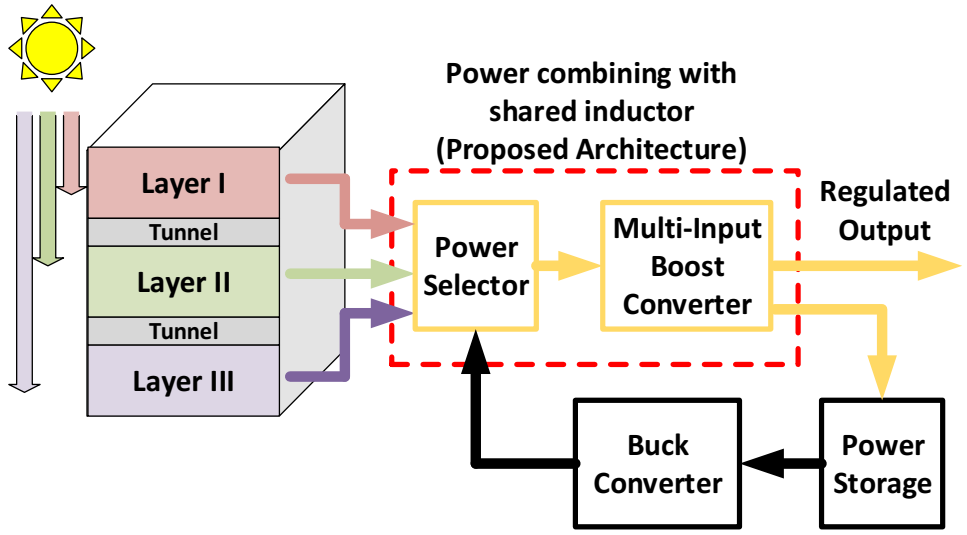

Fig. 1.2. MJ-PV Energy Harvesting System

Chapter 2

PRIOR WORK ON PV ENERGY HARVESTING

2.1 Photovoltaic Cells

A PV cell is essentially a PN junction that directly converts solar energy into electricity. When light shines on a PV cell, it absorbs photons and raise electrons to higher states and therefore generates "light generated current". When the PV cell is connected to external load, it dissipates the energy in the load as shown in Fig. 2.1.

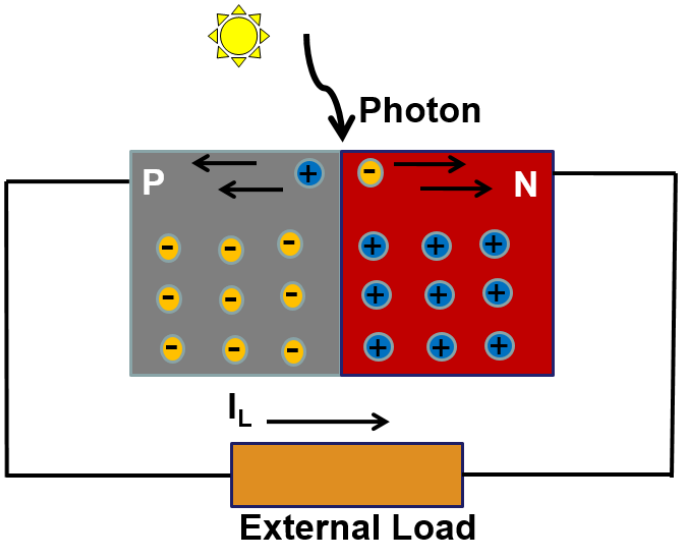

Fig. 2.1 PV Cell Generating Current from Light

PV cells can be modeled as a current source in parallel with a diode and parasitic resistors as shown in Fig. 2.2. Written as I_{SC}, short circuit current is usually considered identical to light generated current, which increases with light intensity. R_{SH} and R_S are parasitic shunt and series resistors respectively. According to the PV diode model, the I-V

curve PV cell can be written as,

$$I_P = I_{SC} - I_0 e^{\frac{q(V+I_P R_S)}{nKT}} - \frac{V+I_P R_S}{R_{SH}} \quad (2.1)$$

where I_0 is dark saturation current of diode, q is elementary charge (i.e.1.602× 10^{-19}), n is ideality factor, K is Boltzmann constant (i.e.1.38064852 × $10^{-23}$$m^2kgs^{-2}K^{-1}$) and T is absolute temperature.

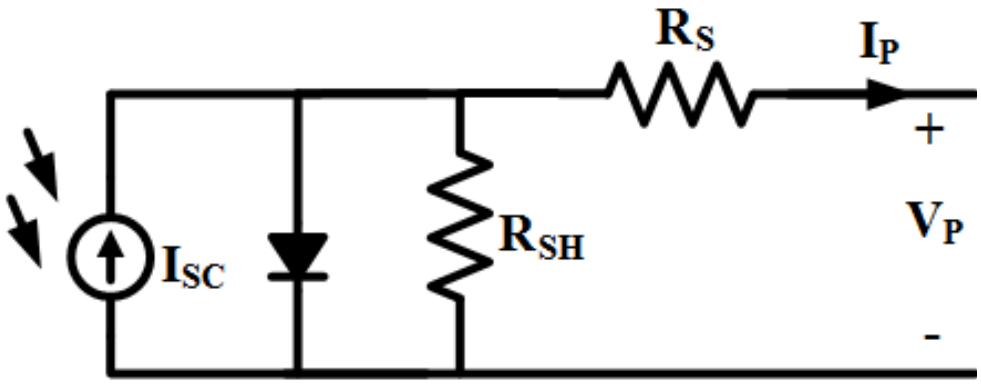

Fig. 2.2 Electric Model of PV Cell

Fig. 2.3 shows the plotted the I-V and P-V curve of a PV cell, where I_{SC} stands for short circuit current, I_{MPP} is the PV output current at its MPP operating condition, V_{MPP} is the PV output voltage at its MPP operating condition and V_{OC} is PV open circuit voltage.

The characteristic resistance R_{CH} of a PV cell is defined as its output resistance at its MPP and can be written as,

$$R_{CH} = \frac{V_{MPP}}{I_{MPP}} \quad (2.2)$$

Only when the resistance of external load is matched to PV characteristic resistance, will maximum power from PV cell be transferred to the load. The PV characteristic changes with environmental factors (such as, temperature and light intensity). Fig. 2.4

shows the P-V curve of a PV cell under different light intensity. Because the MPP changes with environmental factors, dynamic maximum power point tracking (MPPT) is needed to ensure MPP operation.

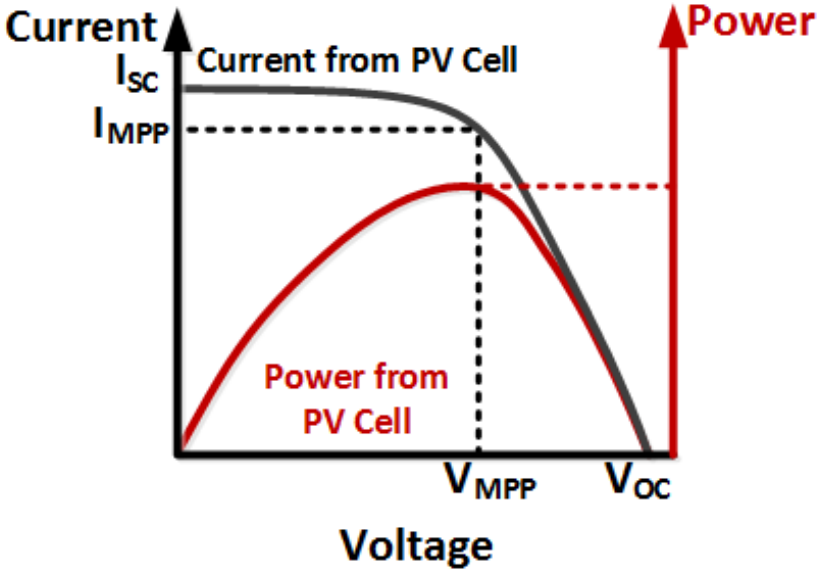

Fig. 2.3 I-V and P-V Curve of a PV Cell

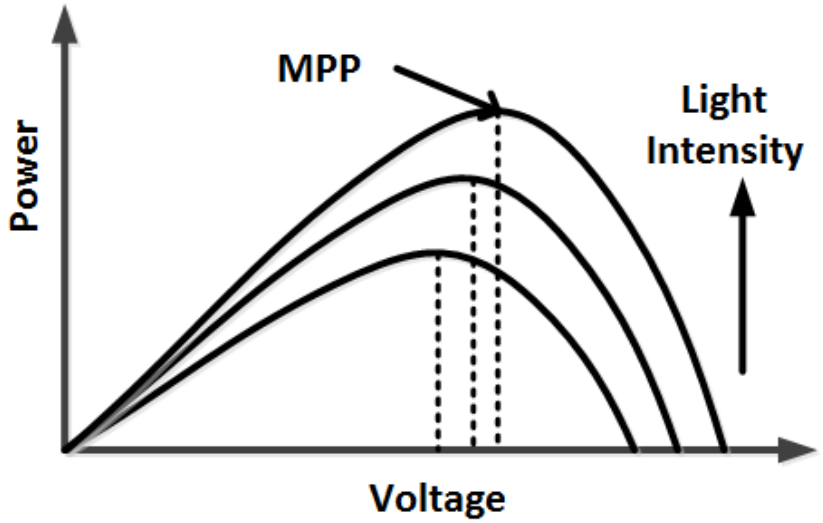

Fig. 2.4 P-V Curve under Different Light Intensity

2.2 Maximum Power Point Tracking

1) Basic Boost Converter Working Principle

Because of the low output voltage of a single PV cell (typically 0.5V), connecting a boost converter between PV cell and load is a common method to achieve cell-level or sub-cell–level MPPT as shown in Fig. 2.5.

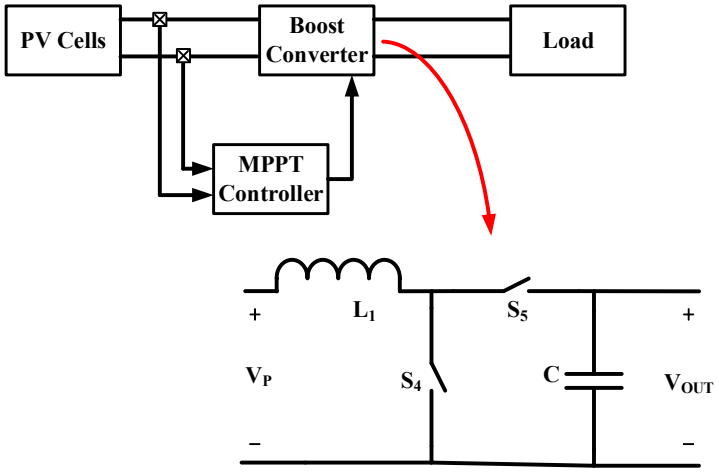

Fig. 2.5 Boost Converter for MPPT

A boost converter consists of an inductor, two switches and an output capacitor. Fig. 2.6 shows the basic working principle of a boost converter.

There are two phases of boost operation. Fig. 2.6 (a) shows that in phase I, S_4 turns on and S_5 turns off. The voltage across inductor is V_P and the input V_P charges inductor. Inductor current increases. Fig. 2.6(b) shows that in phase II, S_4 turns off and S_5 turns on. The voltage across inductor is V_P -V_{OUT} and inductor discharges, delivering power to the load. Fig. 2.6 (c) shows the control signals for both switches, the voltage across inductor V_{L1} and inductor current I_{L1} in both phases. There are generally three types of boost operating mode: CCM, DCM and PCCM. In CCM operation, inductor current is always

above zero, as shown in Fig. 2.6 (c). DCM and PCCM operation will be discussed in section 2.4.

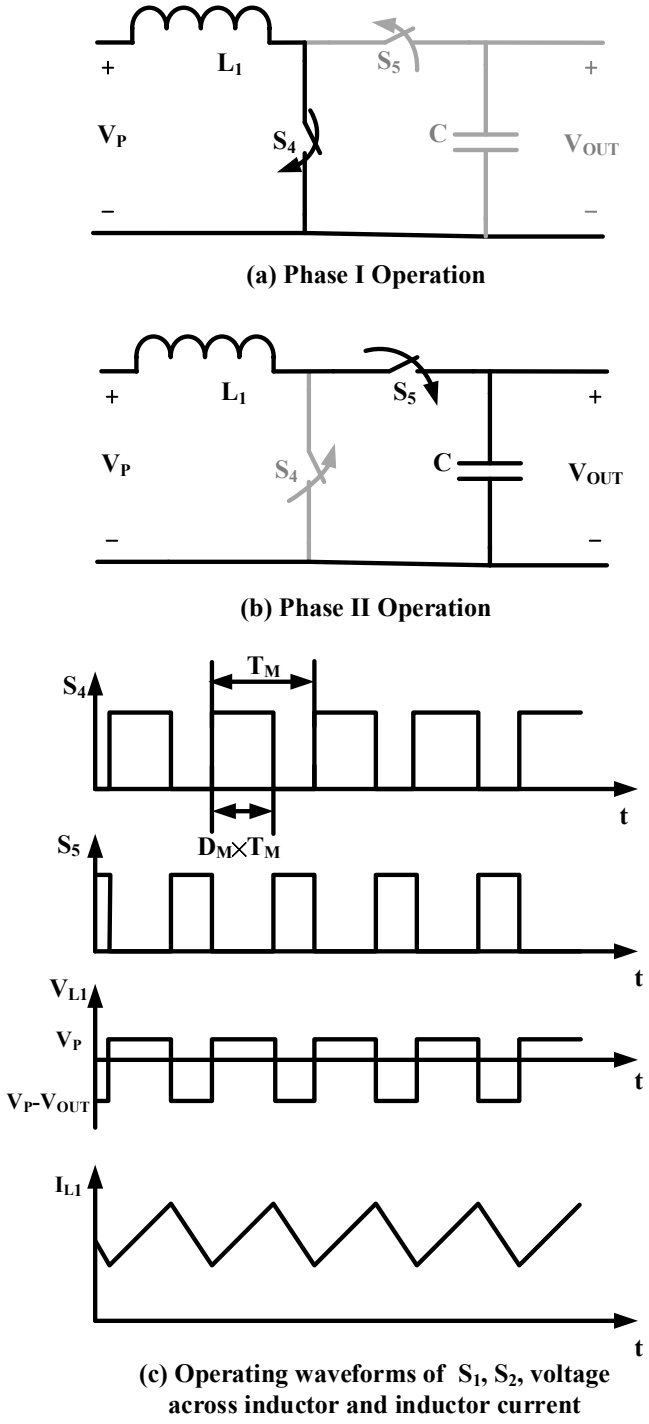

Fig. 2.6 Boost Converter Operating Principle

In CCM operation, inductor current is always above zero, as shown in Fig. 2.6 (c). DCM and PCCM operation will be discussed in section 2.4.

2) Common MPPT techniques

There are many MPPT techniques. Hill climbing, perturb and observe (P&O), ripple correlation control (RCC), incremental conduction are the most common techniques to achieve MPPT without using a microcontroller.

Hill climbing and P&O are similar. Hill climbing perturbs the duty ratio of the power converter, while P&O perturbs the operating voltage of the PV cell. After the perturbation, the output power of PV cell is observed. If the power level increases compared with that before perturbation, then next perturbation will be in the same direction. Otherwise, the perturbation should be in the opposite direction. Fig. 2.7 shows the hill climbing and P&O algorithm operation.

RCC utilizes PV current ripple ΔI_P (or voltage ripple ΔV_P) and power ripple ΔP to control duty ratio D. When current ripple and power ripple are in the same phase (or voltage ripple and power ripple has 180° of phase shift), that is, $\Delta I_P \bullet \Delta P<0$ (or $\Delta V_P \bullet \Delta P>0$), the operating point of the PV cell is on the left side of the MPP (i.e. $V_P<V_{MPP}$ or $I_P> I_{MPP}$). On the other hand, when current ripple and power ripple has 180° of phase shift (or voltage ripple and power ripple are in the same phase), that is, $\Delta I_P \bullet \Delta P>0$ (or $\Delta V_P \bullet \Delta P<0$), the operating point of the PV cell is on the right side of the MPP (i.e. $V_P > V_{MPP}$ or $I_P < I_{MPP}$). According to the polarity of either $\Delta I_P \bullet \Delta P$ or $\Delta V_P \bullet \Delta P$, the controller locates the operating point of the PV cell and with simple and inexpensive analog circuit, MPPT can be achieved. Incremental conductance locates the PV operating point by the slope of P-V curve. When

dP/dV_P is positive, then the operating point is at the left side of MPP (i.e. $V_P<V_{MPP}$); when dP/dV_P is negative, then the operating point is at the right side of MPP (i.e. $V_P>V_{MPP}$).

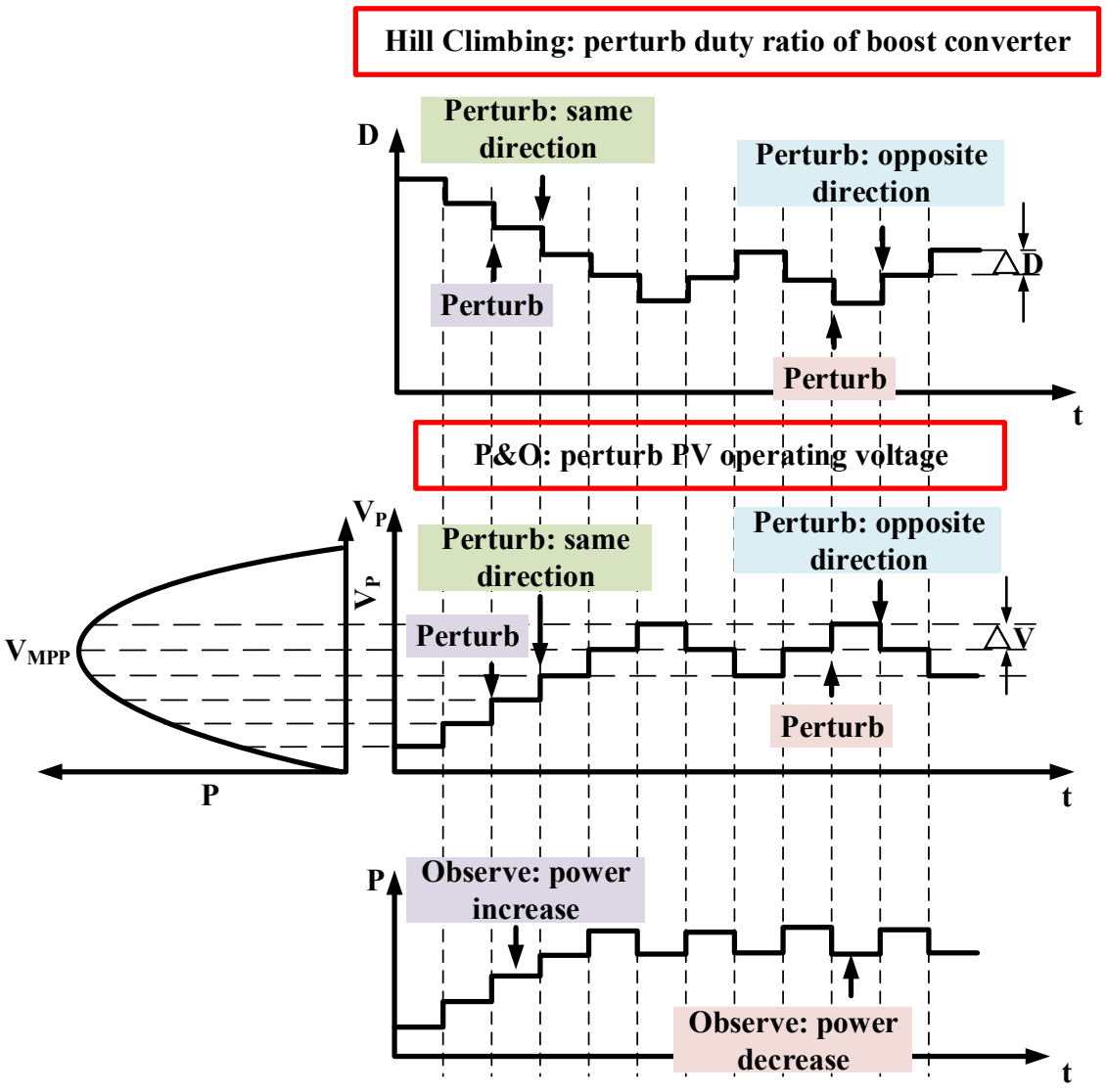

Fig. 2.7 Hill Climbing and P&O Algorithm

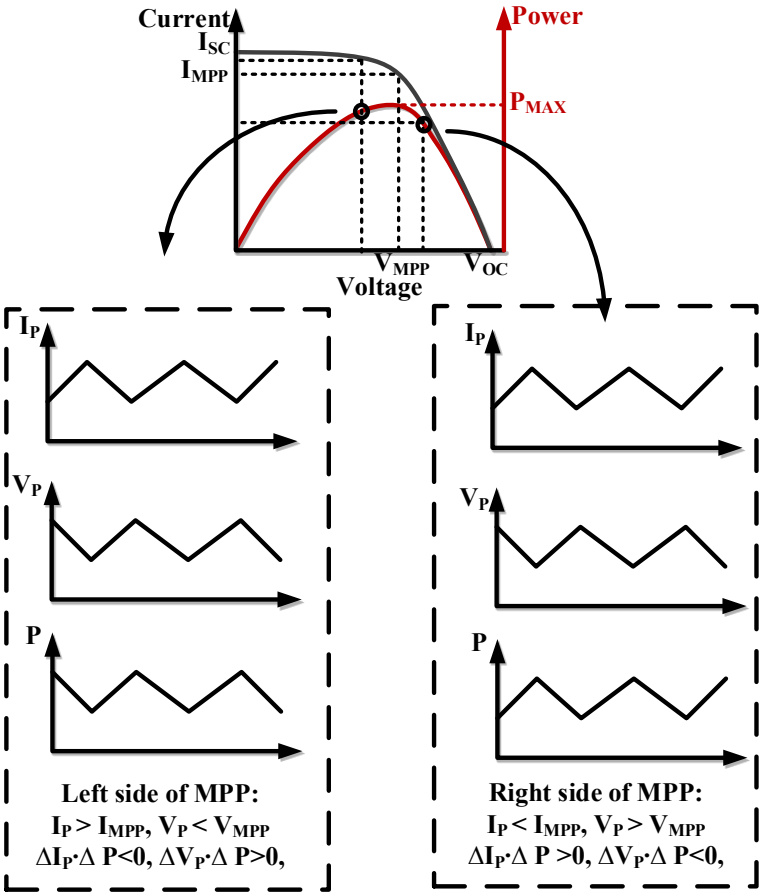

Fig. 2.8 RCC Algorithm

Because

$$R_{Load}(1-D)^2 = D_1 \frac{V_{P1}}{I_1} + (1-D_1)\frac{V_{P2}}{I_2} \tag{2.3}$$

$dP/dV_P>0$ can be written as $dI/dV_P>-I/V_P$, and similarly, $dP/dV_P<0$ can be written as $dI/dV_P<-I/V_P$. Incremental conductance of the PV cell is defined as dI/dV_P and instantaneous conductance is defined as I/V_P. Incremental conductance algorithm achieves MPP by matching PV instantaneous conductance with its incremental conductance.

2.3 Output Regulation

As discuss above a boost converter is connected between PV cells and the load for MPPT. To attain a well-regulated DC output, another DC-DC converter is needed for output regulation as shown in Fig. 2.9.

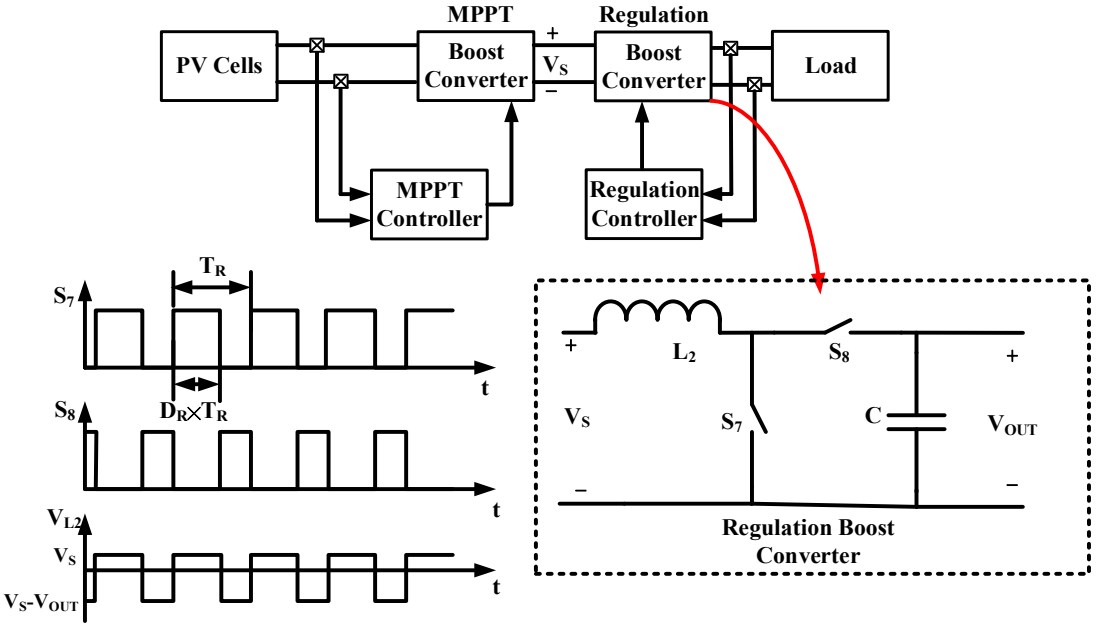

Fig. 2.9. Boost Converter for MPPT and Output Regulation

After the first boost converter, an unregulated voltage V_S is generated at the input of the regulation boost converter. Apply inductor volt-sec balance principle,

$$V_S \cdot D_R + (V_S - V_{OUT})(1 - D_R) = 0 \tag{2.4}$$

Therefore,

$$V_{OUT} = \frac{V_S}{1-D_R} \tag{2.5}$$

Where D_R is the duty ratio of the regulation boost converter. There are many control schemes for a boost converter to regulate its output voltage. The most used control schemes

are voltage mode control, current mode control.

In voltage control mode, a type III compensator is usually used in boost converters operating in CCM, and a type II compensator is usually used in boost converters operating in DCM. Compared to voltage control mode, current control mode has the advantages of easier compensator design and fast transient response.

Other control schemes such as, hysteresis control and constant-on time control, are also widely used.

2.4 Prior Work on Multi-Input, Inductor Time-Sharing Boost Converters

1) Using diode between sub-cells and inductor

In [16], multiple PV panels are connected to converter input through diodes and power switches driven by overlapping control signals. Due to the diodes, during the overlapping time, only the path from the power source with higher voltage to the converter would be enabled. This solution eliminates ringing during the dead time, at the input node when switching between input sources. However, it is not suitable for cell-level (or sub-cell level) power management due to the large voltage drop across diode.

2) DCM and PCCM operation

Fig. 2.10 shows the inductor current waveform of DCM and PCCM. In DCM, inductor current goes to zero at the end of every cycle, as shown in Fig. 2.10(a). PCCM operation is similar to DCM but instead of zero, the current stops decreasing at a pre-determined positive current level and stays at that current until the next cycle, as shown in Fig. 2.10 (b). In [14], an energy harvesting system combining power from three different

renewable energy sources, including PV cells, is presented. The converter operates in DCM and achieves peak power-efficiency of 83% at 1 mW input PV power. However, when the power level is higher, such as a few hundred milli-watts, DCM will bring very high current ripple, which causes extremely low efficiency, especially when the inductor is being time shared. In [17], the converter operates in PCCM. PCCM decreases the current ripple compared to DCM. However, neither DCM nor PCCM operation of the converter provide good efficiency when the current levels of inputs are widely spread. For MJ-PV cells, the current and voltage differences of the inputs are large and operating the converter in CCM (continuous conduction mode) would provide better power efficiency.

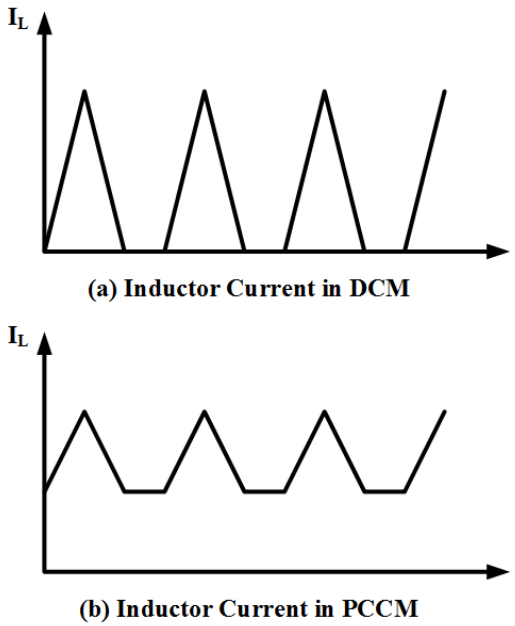

Fig. 2.10 Inductor Current Waveform in DCM and PCCM

Chapter 3

PROPOSED SINGLE-INDUCTOR DC-DC CONVERTER ENERGY HARVESTER

3.1 Challenges of Inductor Time-Sharing for MJ-PV Cells

One of the challenges of inductor time-sharing DC-DC converters operating in CCM for harvesting energy from MJ-PV cells is input cross-regulation. Here, input cross-regulation describes the change in voltage on one input source caused by the voltage change on another input source. Conventional DC-DC converter designs assume ideal power sources that provides a stable output voltage at any current levels. However, this assumption is no longer valid when the inputs are PV cells. As observed from I-V curve of PV cells in Fig.1.1, PV output voltage is not constant, but a function of terminal current and the maximum power is obtained at a particular operating condition.

Inductor time-sharing DC-DC boost converter with two-layer MJ-PV input is shown in 3(a). Inductor L, switches S_4 and S_5, and load capacitance C_L form the boost converter. Load is represented by R_{Load}. The converter is connected to sub-cell I and sub-cell II through switches S_1 and S_2, respectively. S_1 and S_2 are ON for D_1T_{IN} and D_2T_{IN} durations, respectively in every period T_{IN}, as shown in 3(b). Applying capacitor amp-second balance principle on C_1 and C_2, average inductor current (I_L) is expressed as,

$$\begin{cases} I_L = I_1/D_1 \\ I_L = I_2/D_2 \end{cases} \tag{3.1}$$

where, I_1, I_2 are average current of sub-cell I and sub-cell II, respectively. Assuming $D_1 + D_2 = 1$, I_1 is written as,

$$I_1 = \frac{D_1}{1-D_1} I_2 \tag{3.2}$$

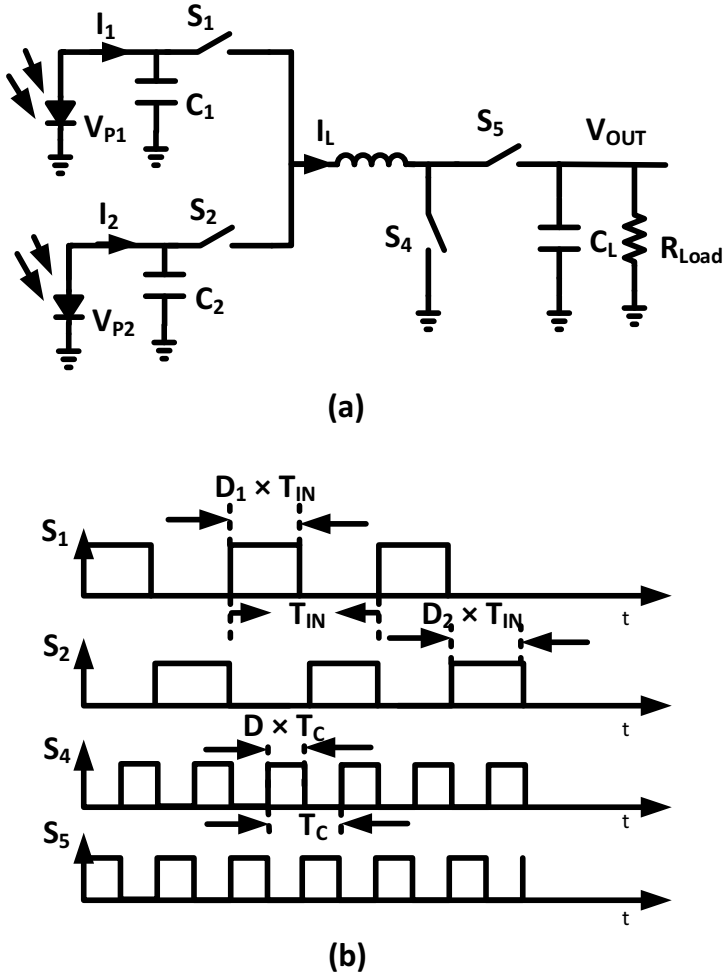

Fig. 3.1(a) Inductor Time-Sharing DC-DC Converter and (b) Switch Control Signal

As shown in (2), I_1 and I_2 are correlated, hence sub-cell output voltages (V_{P1} and V_{P2}) are correlated as well, and cross-regulation occurs.

Assuming converter operates in CCM with switching period of T_C. The average input impedance of the converter is $R_{Load}(1\text{-}D)^2$. At steady-state condition, boost converter input impedance is equal to the equivalent output impedance of the MJ-PV cell, and can be expressed as

$$R_{Load}(1-D)^2 = D_1\frac{V_{P1}}{I_1} + (1-D_1)\frac{V_{P2}}{I_2} \tag{3.3}$$

As shown in (3.3), the MPPT controller needs to control both D and D_1, to achieve MPP conditions ($V_{P1,MPP}$, $I_{1,MPP}$, and $V_{P2,MPP}$, $I_{2,MPP}$) for both sub-cells, while conventional MPPT algorithms for SJ-PV cells controls only converter duty ratio D. Therefore, when there is input cross regulation, the conventional MPPT algorithms would not work and it would require complicated algorithms and control circuits to achieve MPPT for an inductor time-sharing architecture operating in CCM for MJ-PV cells.

This work has focused on reduction of input cross regulation in CCM operation. Inductor current cannot change instantaneously, and any change in one input current will be coupled to the inductor current, and then coupled to the other input when switching among inputs, as shown in (1), (2). In the proposed architecture, a hysteresis current controller is used to regulate the inductor current, so that it always remains the same regardless of any change of the inputs. Second, the operating conditions of two inputs are coupled through D_1 and D_2, because the S_1 and S_2 are controlled by complementary signals, as shown in (2). In this design, an additional power switch S_3 is used across the inductor to decouple D_1 and D_2. This will be explained in later sections.

3.2 System Structure

The proposed single inductor DC-DC boost converter architecture for two-layer MJ-PV cell is shown in Fig. 3.2. The system consists of three feedback loops controlling input stage, converter stage and output stage. The MPPT controller senses power from both PV sub-cells, and controls input switches S_1 and S_2 based on hill climbing algorithm. The time-sharing controller decides ON time for S_3 in a period of T_{IN}. The current controller regulates inductor current with S_4 and S_5/S_6 using current mode hysteresis. The output regulator loop provides output voltage regulation at V_{OUT} controlling S_5 and S_6 using voltage mode hysteresis.

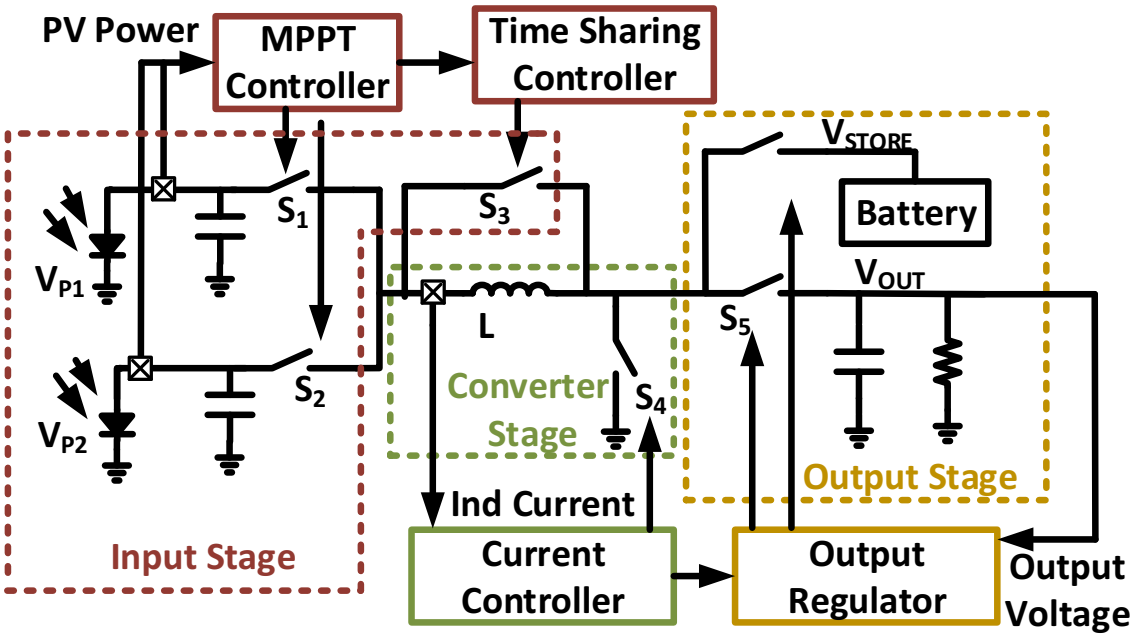

Fig. 3.2 Proposed Inductor Time-Sharing DC-DC Boost Converter

3.3 Converter Stage

As discussed above, one of the main causes of cross-regulation in time-sharing converter is inductor current coupling. Although input cross-regulation can be reduced in DCM and PCCM operation by always switching from one input source to another when inductor current is zero or at a constant value, DCM and PCCM causes poor efficiency, especially in MJ-PV application.

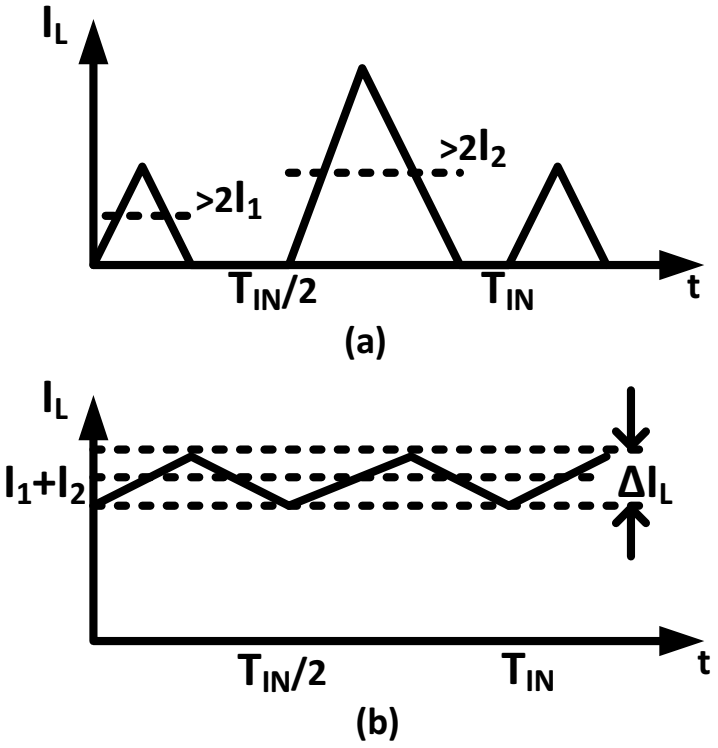

Fig. 3.3 Time-Sharing Inductor Current (a) in DCM, and (b) in CCM

Fig. 3.3 shows the inductor current of DCM and CCM operation (For simplicity, assuming $D_1=D_2=0.5$). Assuming $2I_1 = I_2 = 2I$, the minimum conduction loss of the

converter when operating in DCM is written as,

$$P_{LOSS,DCM,Min} = \frac{1}{2}\left[(2I_1)^2 + \frac{(4I_1)^2}{12} + (2I_2)^2 + \frac{(4I_2)^2}{12}\right](R_L + R_{ON})$$

$$= \frac{40}{3}I^2(R + R_{ON}) \approx 13.33I^2(R + R_{ON}) \quad (3.4)$$

where, R_L and R_{ON} are inductor series resistance and switch ON-resistance, respectively. The conduction loss of converter operating in CCM is expressed as,

$$P_{LOSS,CCM} = \left[(I_1 + I_2)^2 + \Delta {I_L}^2/12\right](R_L + R_{ON}) \quad (3.5)$$

where, ΔI_L is the inductor current ripple. Assuming 100% inductor current ripple (i.e. $\Delta I_L = I_1 + I_2$), the $P_{LOSS,\ CCM}$ is written as,

$$P_{LOSS,CCM} = \frac{39}{4}I^2(R_L + R_{ON}) \approx 9.75I^2(R_L + R_{ON}) \quad (3.6)$$

Comparing (3.4) and (3.6), the minimal power loss in DCM is much larger than that in CCM.

In this work, to eliminate cross-regulation in CCM, a current controller, as shown in Fig. 3.4, is used to regulate the inductor current so that the change in inputs does not affect the inductor current and therefore reduces the cross-regulation. The controller consists of an inductor current sensor and a hysteresis comparator, as shown in 6(a). The sensed inductor current is compared with a maximum value I_{High} and a minimum value I_{Low} using the hysteresis comparator, and the output of the comparator controls low-side switch S_4 of boost converter to regulate I_L within the hysteresis window as shown in 3.6(b). The control signal is also used for output regulation, which will be discussed in 3.6.

3.4 Input Stage

A free-wheel switch S_3 is added across the inductor as shown in Fig. 3.2 to suppress cross-regulation caused by complementary control signals (i.e. $D_1 + D_2 = 1$) for input switches S_1 and S_2.

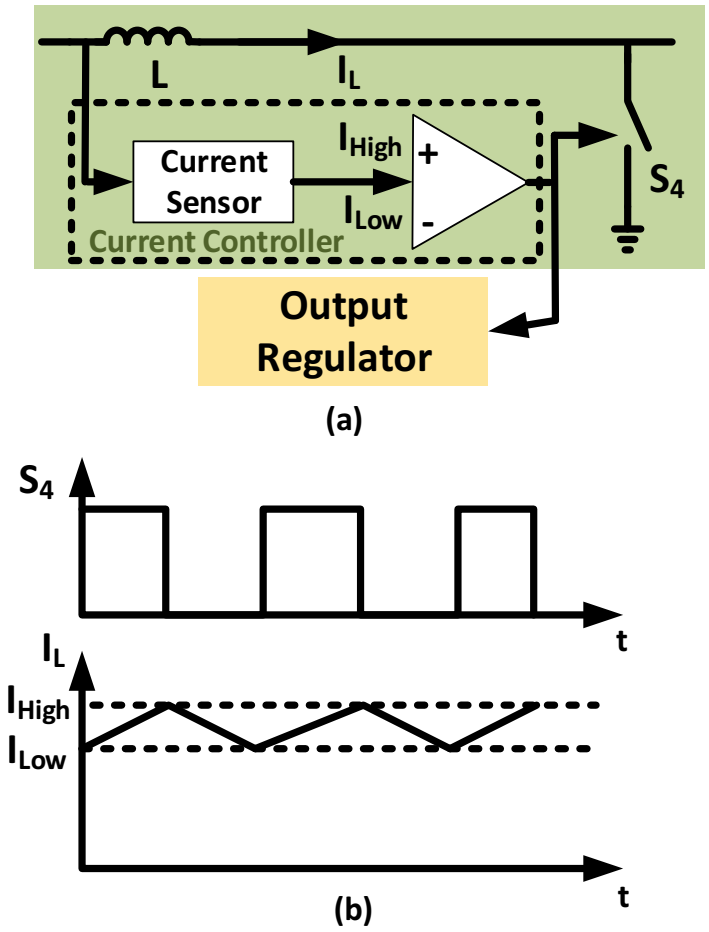

Fig. 3.4 (a) Inductor Current Controller, and (b) Control Signal for S_4 and Inductor Current

The inductor time-sharing in T_{IN} period is shown in Fig. 3.5(a). Switch S_1 is ON for D_1T_{IN} duration in every T_{IN} period and the converter harvests energy from MJ-PV sub-cell

I as shown in Fig. 3.5(b). As shown in Fig. 3.5(c), the converter harvests energy from MJ-PV sub-cell II for D_2T_{IN} duration in every T_{IN} period when S_2 is ON. When S_3 is ON, the inductor freewheels, storing energy in the inductor as shown in Fig. 3.5(d). The inductor time-sharing controller consists of simple logic gates used to generate S_3 from S_1 and S_2, so that $D_1 + D_2 + D_3 = 1$.

3.5 MPPT Controller

Together, the inductor current regulation and inductor time-sharing scheme, reduce input cross-regulation significantly. Thus, the operating condition of each input PV sub-cell can be controlled almost independently. Conventional hill climbing algorithms usually perturb the converter duty ratio to track MPP. In this work, notice from (1) and (2) that since I_L is a regulated constant, I_1 is a linear function of D_1 and similarly, I_2 is a linear function of D_2. Hence, by perturbing D_1 and D_2, instead of boost duty cycle D, MPPT can be achieved by directly controlling the PV sub-cell currents. The small variation of converter operating condition due to the perturbation in D_1 or D_2 and transferring from one sub-cell to another, is adjusted by the fast hysteresis inductor-current controller loop, hence achieving MPPT faster.

The flow chart of hill climbing algorithm is given in Fig. 3.6(a). The algorithm works based on perturb-and-observe (P&O) principle. Here, duty-ratio (either D_1 or D_2) is perturbed and PV sub-cell output power is observed. As shown in Fig. 3.6(b), the MPPT controller compares the output of PV power monitor with its output from previous cycle. Based on the comparison, an incremental or decremental signal will be applied to the duty

ratio of input switch control signals. If the monitored power is greater than the previous cycle, then the duty ratio will be perturbed in the same direction as before. Otherwise, it will be perturbed in the opposite direction. Finally, clock signals are generated by PWM generators to control the input switches S_1 and S_2.

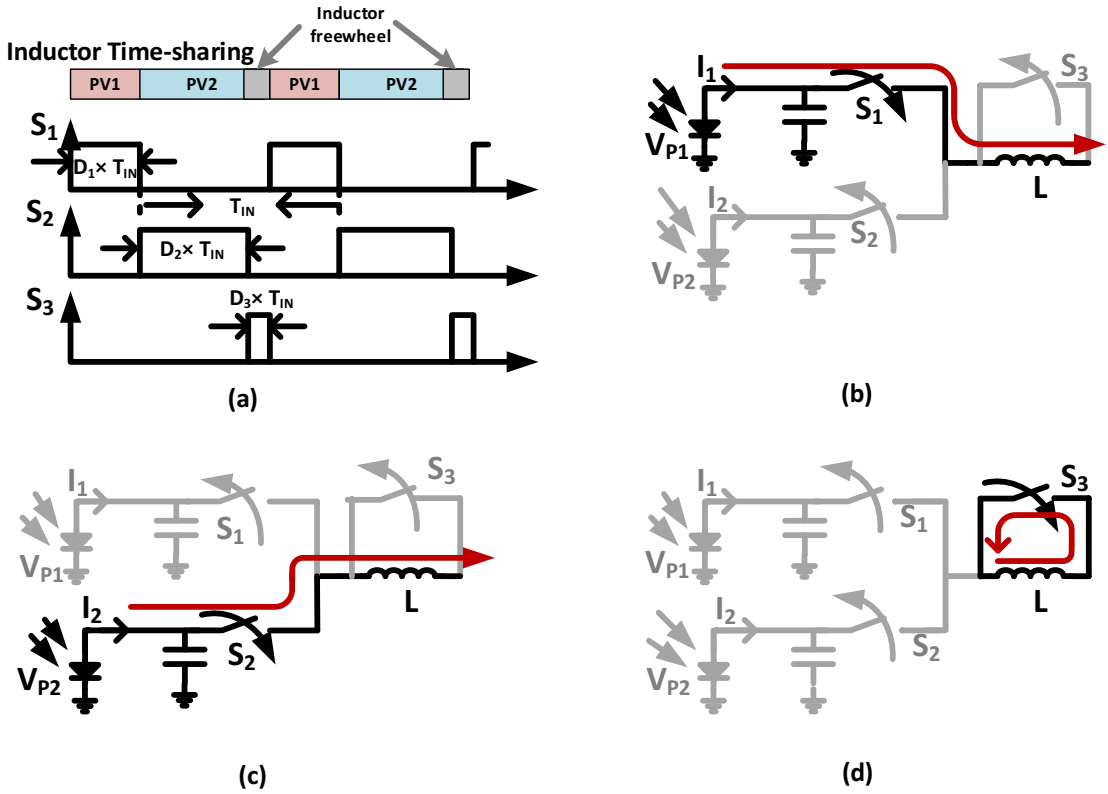

Fig. 3.5 (a) Control Signals for S_1, S_2 and S_3. Converter Current Paths: (b) Sub-cell I, (c) Sub-cell II, and (d) Free-wheel

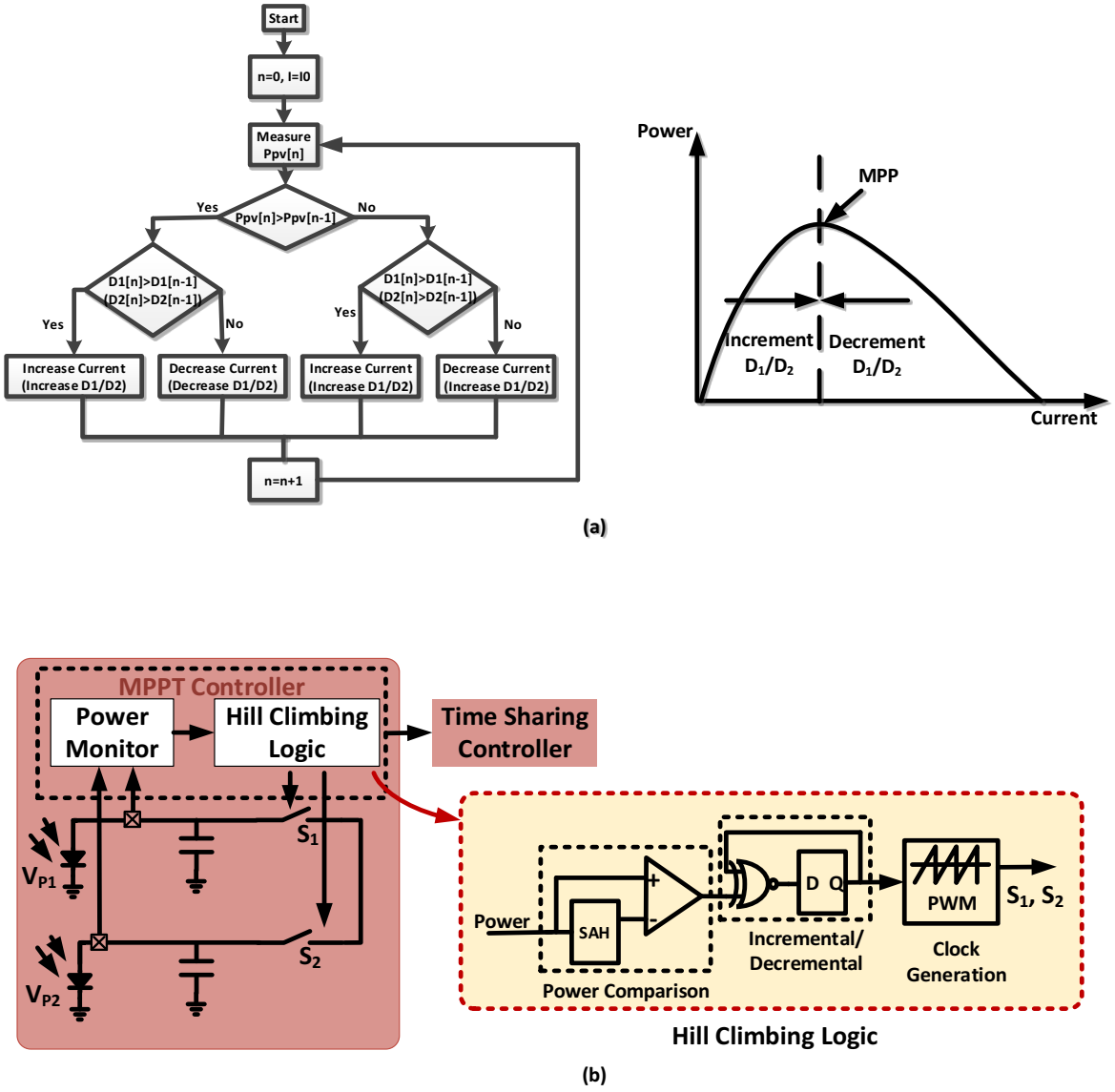

Fig. 3.6 (a) Hill Climbing Algorithm Flow Chart, and (b) MPPT Controller Implementation

3.6 Output Regulation

As shown in Fig. 3.7, the output stage has two paths: one primary path and one secondary path.

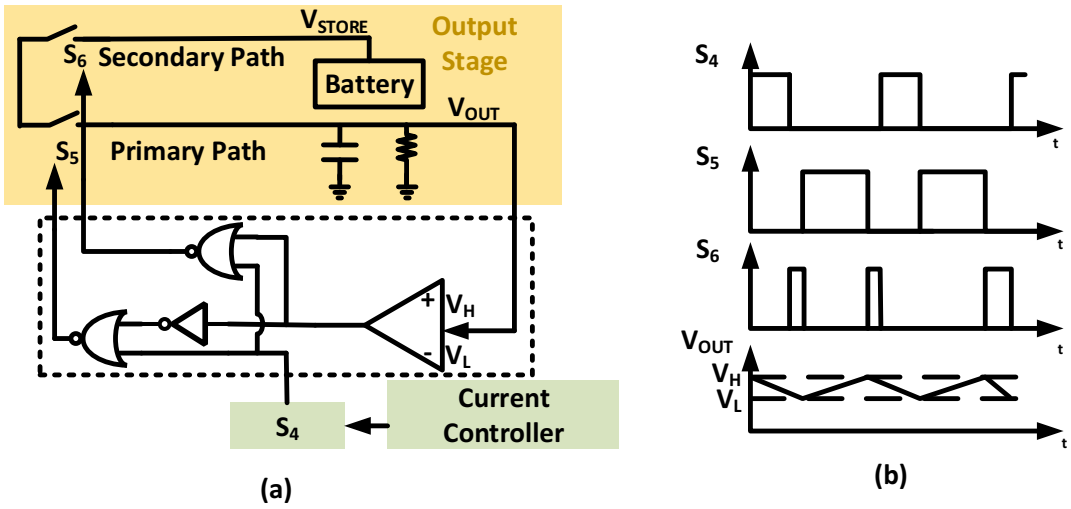

Fig. 3.7 (a) Output Voltage Regulation Loop, and (b) V_{OUT} and Control Signals for S_4, S_5 and S_6.

A hysteresis comparator monitors the output voltage, compares it to the two references V_H and V_L and enables either primary path or secondary path:

(1) When output is lower than V_L, the primary path will be enabled. S_5 turns on whenever S_4 is off and S_6 will be disabled. The input power will be delivered to the load.

(2) When output is higher than V_H, the secondary path will be enabled. S_6 turns on whenever S_4 is off and S_5 will be disabled, the power will be delivered to and stored in the battery.

Therefore, the hysteresis control loop provides regulated output voltage by storing extra input energy that load doesn't require, to battery storage.

Chapter 4

CIRCUIT DETAILS

4.1 Inductor Current Sensor

Inductor current sensing is necessary for any DC-DC converter controlled in current mode. A series resistor (for current sensing) causes significant power loss. Mirroring current from power switches to sense the inductor current is a common technique used to avoid series resistors. As shown in Fig. 3.5, inductor is time shared between S_1, S_2 and S_3. Therefore, the inductor current can be sensed from power switches S_1, S_2 and S_3. Fig. 4.1(a) shows the current sensing circuit of S_1. Two identical mirror switches S_{M1} and M_1 are connected in series and then in parallel with S_1. The ratio between mirror switches and power switch S1 is 1:640. A common gate amplifier provides a small bias current I_B at its inputs. The feedback loop ensures the same voltage at the node V_A and V_B. M_1 and M_2 are identical and both operates in linear region. Therefore,

$$I_{M1} = I_{M2} \tag{4.1}$$

$$I_{M9} = I_{M2} - I_B = I_{M1} - I_B = I_{M\_S1} \tag{4.2}$$

Similarly, current through S_2 and S_3 can be sensed in the same way. Since S_1, S_2 and S_3 are complementary. The mirror switch M_1 and the op-amp can also be time-shared.

Fig. 4.1(b) shows the complete implementation of the current sensor. The mirrored current of three switches sums up at node V_A. The sensed inductor current through M_9 is written as,

$$I_M = \frac{1}{1280} I_L \tag{4.3}$$

The ratio between M_9 and M_{10} is K_2:1. M_{11} and M_{12} has the same size. Therefore, the sensor output voltage V_S is expressed as,

$$V_S = V_{DD} - \frac{1}{2K_1K_2} I_L R \tag{4.4}$$

In the design, values of K_1 and K_2 are 640 and 4, respectively.

A cross-coupled common-gate amplifier is used as A_0. Transistors M_3-M_8, and current sources I_{B2} form A_0 amplifier. Input cross-coupled pair (M_4-M_5) provides fast transient response required for inductor hysteresis current loop.

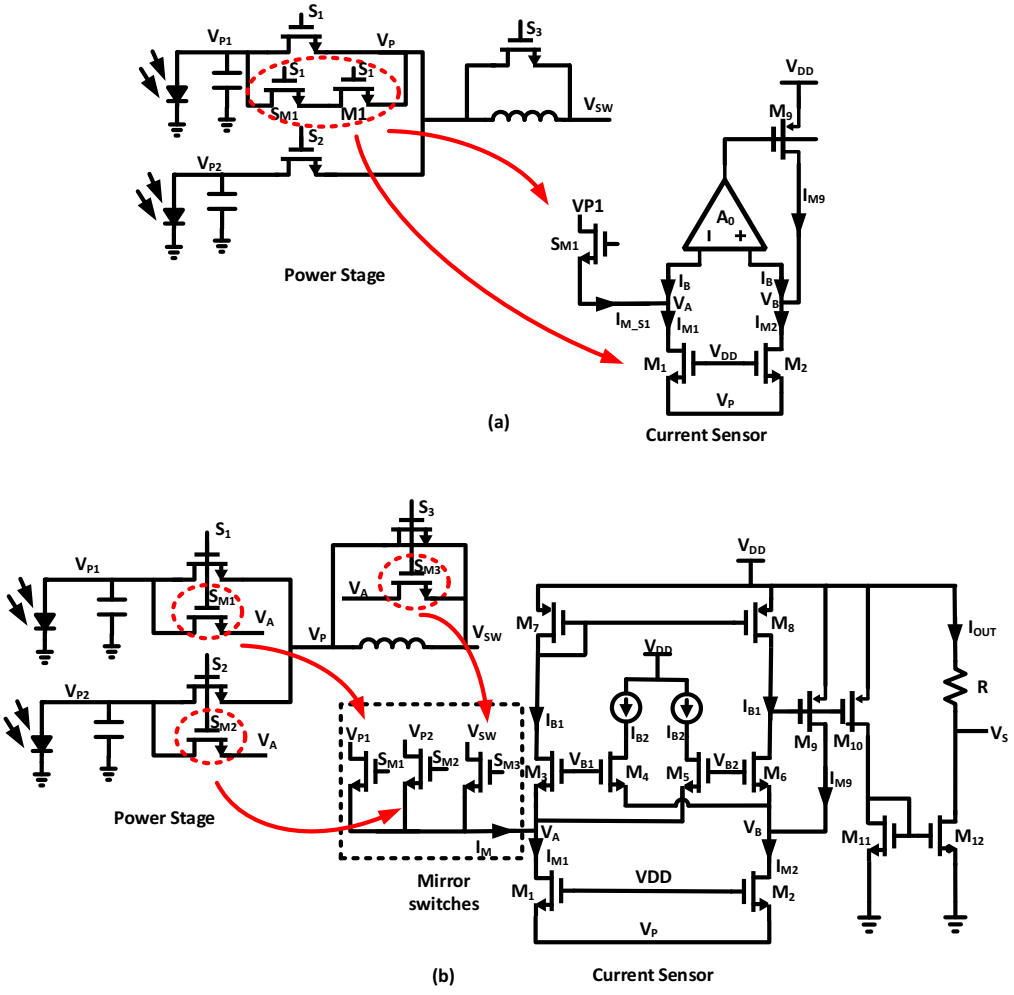

Fig. 4.1 (a) Current Sensor for S1, and (b) Inductor Current Senso

4.2 Power Monitor

As discussed before, for MPPT, PV power monitoring is necessary. Traditional analog power monitors usually employ power-hungry current sensors on power paths. A time-based power monitor is designed as shown in 11, and the basic concept is taken from [18].

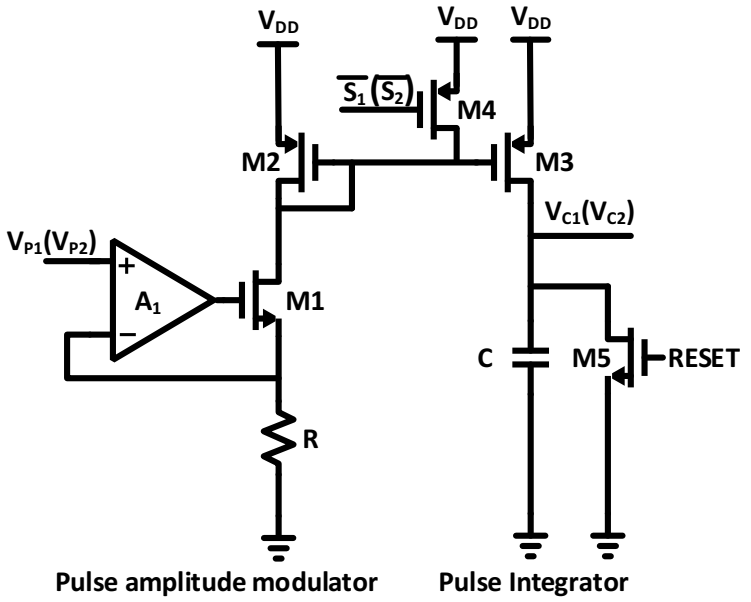

Fig. 4.2 Power Monitor Circuit

The power monitor consists of a pulse amplitude modulator (PAM), a pulse integrator (PI), and a switch M_4. The PAM is formed by an op-amp, a resistor R, and transistors M_1-M_3. The PAM converter the PV voltage information into current. The PI consists of a capacitor C. The ON time of M_4 controls the integration time. The duty-ratio (D_1, D_2) of S_1 and S_2 control signals carry information of current (I_1, I_2) through S_1 and S_2 switches. Thus, the PI calculates instantaneous PV power represented by voltage V_C across

C. Switch M_5 connected across C resets the power monitor at the beginning of every MPPT cycle.

Using (3.1), the outputs (V_{C1} and V_{C2}) of the power monitors used for sub-cell I and sub-cell II are expressed as,

$$\begin{cases} V_{C1} = \frac{V_{P1}D_1T_{IN}}{RC} = \frac{V_{P1}I_1T_{IN}}{RCI_L} \propto V_{P1}I_1 \\ V_{C2} = \frac{V_{P2}D_2T_{IN}}{RC} = \frac{V_{P2}I_2T_{IN}}{RCI_L} \propto V_{P2}I_2 \end{cases} \tag{4.5}$$

4.3 Sample and Hold Block

In any hill climbing or P&O algorithm implementation, sample and hold block is essential to store the PV power information from the previous cycle. When the PV operating point is close to its MPP, the power difference ΔP become smaller and smaller. Therefore, the accuracy of the sample and hold block is crucial. If the accuracy is poor, the oscillation around the MPP will be larger and causes the MPPT efficiency to decrease. Since each MPPT cycle is typically from a few hundred micro-seconds to a few milli-second, the sample and hold block need to hold the power information for a long time.

Fig. 4.3 shows the implemented sample and hold circuit. Two transmission gate T_1 and T_2 between input and output reduces leakage. The transmission gate T_3 turns on during the hold time and the op-amp in unity gain feedback ensures that the voltage across T_2 is the zero and therefore further decreases the leakage. This sample and hold topology is able to hold the PV power information for seconds.

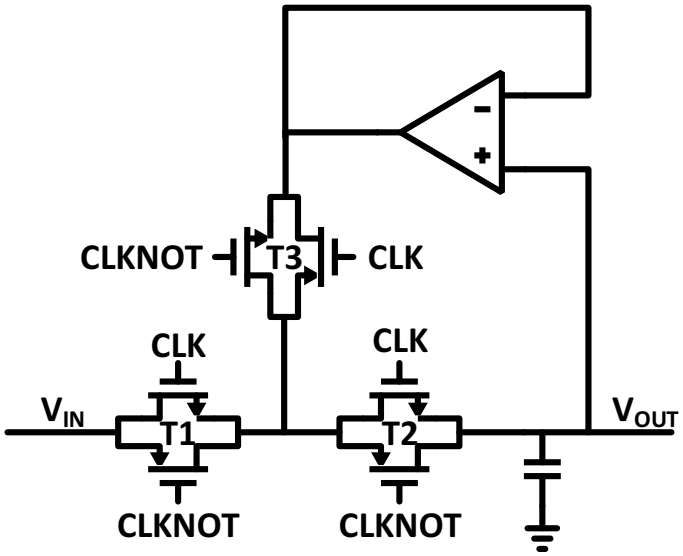

Fig. 4.3 Sample and Hold Circuit

Chapter 5

EXPERIMENTAL RESULTS

The proposed system was implemented in standard 0.18-um CMOS process. The die microphotograph is shown in Fig. 5.1. The power switches and control circuits occupies silicon area of 1.5mm×3mm.

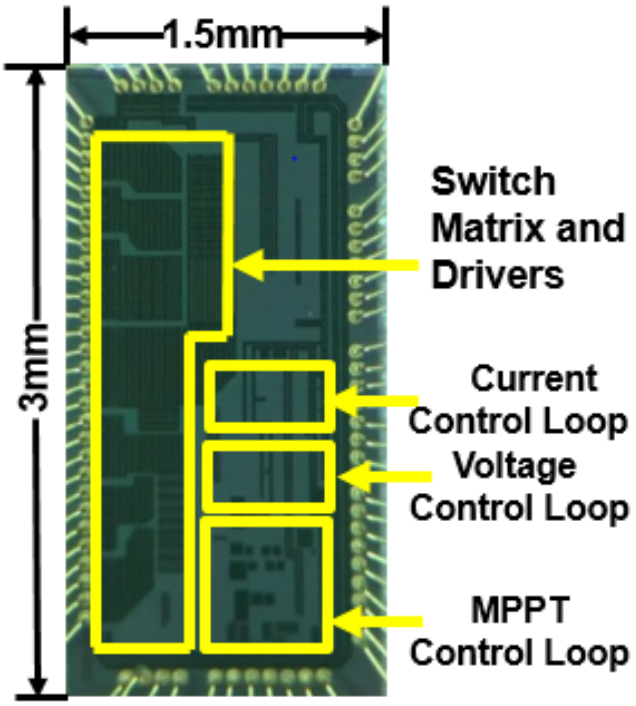

Fig. 5.1 Die Microphotograph

5.1 Test Board and Measurement Setup

A test board is designed for the measurement of this IC as shown in Fig. 5.2. Two different PV cells are used as input sources to mimic the sub-cells of a MJ-PV. A 1F super-capacitor is used as power storage on the secondary path at V_{STORE}. An 8.2uH inductor is

used. A 10uF input capacitor was placed at each PV cells. At full light intensity, the two PV cells generates around 8mW and 59mW of power, respectively.

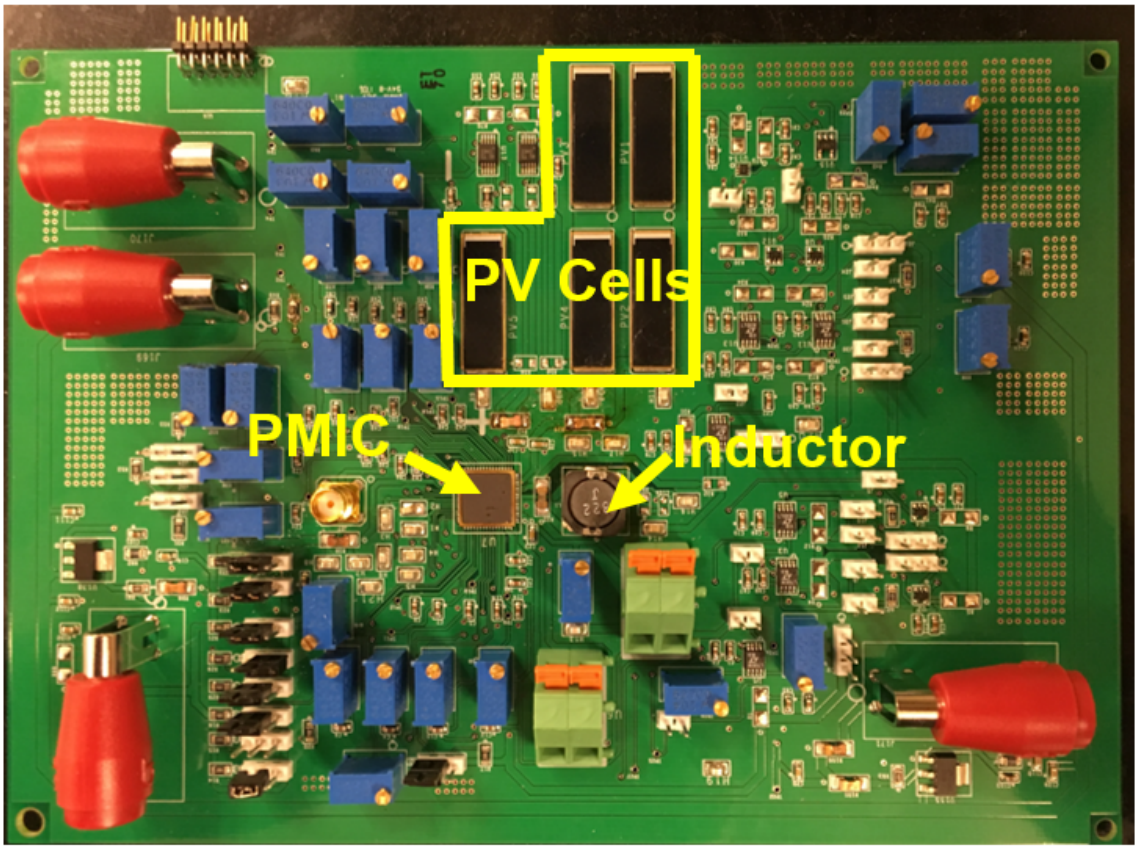

Fig. 5.2 Test Board

5.2 Top-level Measurement Results

Fig. 5.3 shows the measurement result of inductor time-sharing. The input switches S_1, S_2 and the free-wheeling switch S_3 operates at approximately 100 KHz. As shown in Fig. 5.3, the inductor is being time-shared by these three switches. During S_1, the PV sub-cell I is enabled and the converter input node V_P follows sub-cell I output voltage V_{P1}. During S_2, the PV sub-cell II is enabled and the converter input node V_P follows sub-cell

II output voltage V_{P2}. During S_3, inductor free-wheels and the converter input node is set to zero. This is because switch S_3 is implemented by a NMOS transistor, setting V_P to zero minimizes the ON-resistance of the switch.

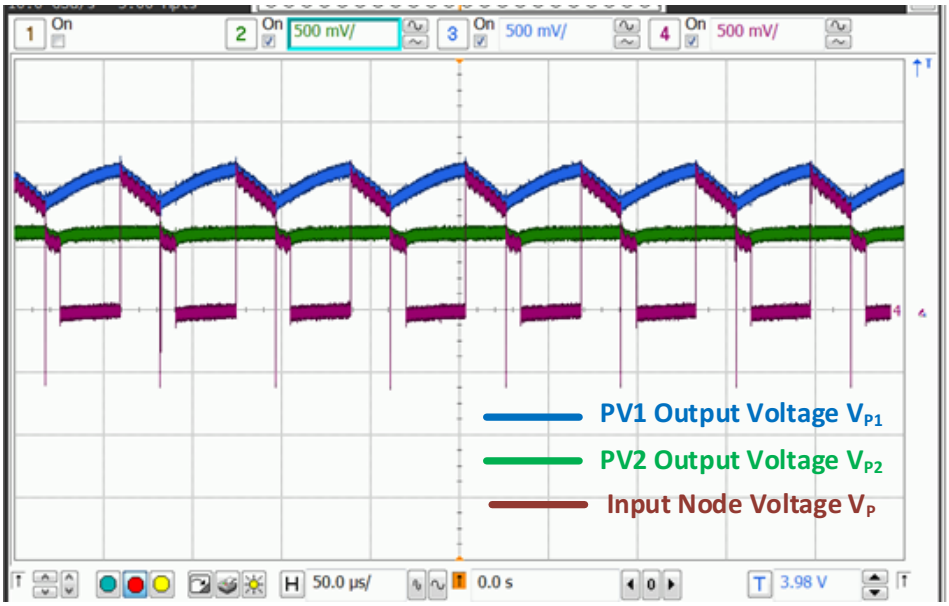

Fig. 5.3 Inductor Time-Sharing

The output of the primary path (i.e. external load) is regulated at 1.8V and the output of secondary path (i.e. super-capacitor) is set at around 2V.

Fig. 5.4 shows the measured efficiencies. For efficiency measurements, V_{STORE} is set to 1.8V. The total output power is measured as the sum of the power to V_{LOAD} and V_{STORE}. The converter achieves peak efficiency of around 85% at full load.

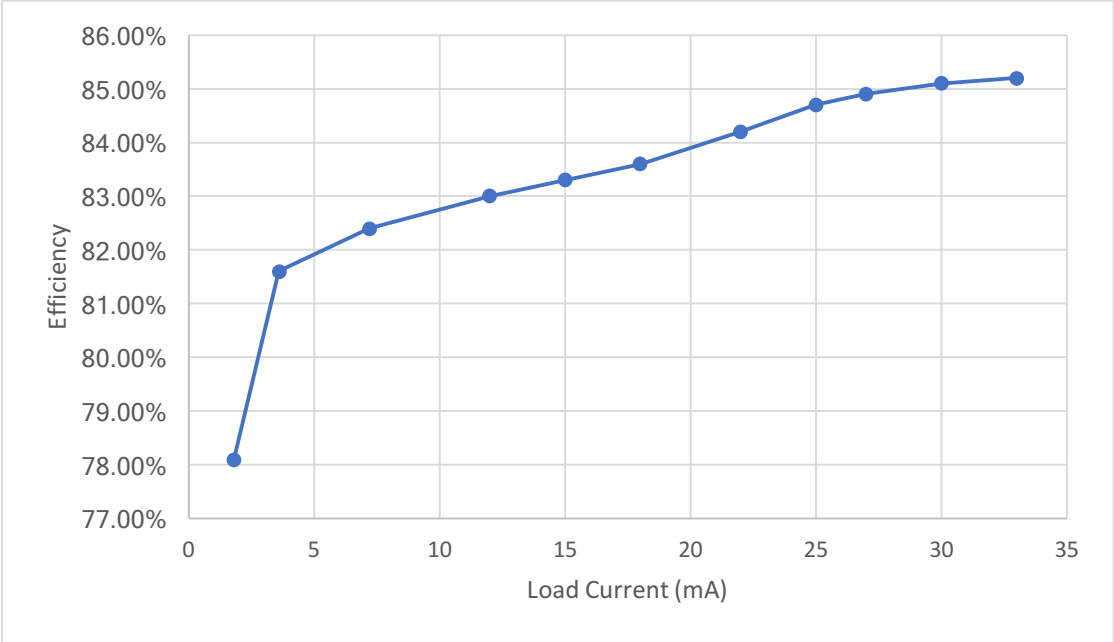

Fig. 5.4 Measurement Efficiency under Different Load Conditions

5.3 Current Regulation Loop Measurement Results

Fig. 5.5 shows the measurement result of the inductor current regulation. The inductor current is regulated at around 200mA. The inductor current is well-regulated in all three phases (sub-cell I enabled, sub-cell II enabled, and inductor freewheel). Notice from (4.4), the inductor current sensor output and the inductor current is in inverting phase. As can be seem in Fig. 5.5, when sub-cell I or sub-cell II are enabled, the inductor current is regulated within the hysteresis window; and when inductor current free-wheels, inductor current slightly decreases due to the conducting resistance of the free-wheeling switch S_3.

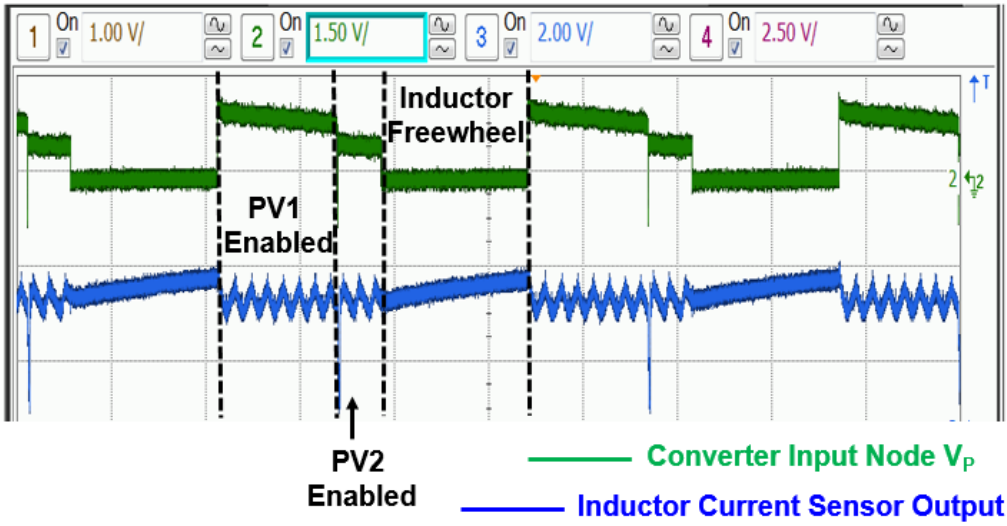

Fig. 5.5 Converter Stage Measurement Results

5.4 MPPT Transient

The duty ratio of the input clocks are measured at different light intensity to verify the functionality of MPPT as shown in Fig. 5.6. The MPPT functionality can be characterized as the relationship between light intensity and duty ratio of input clocks. When light intensity is low, as shown in Fig. 5.6 (a), MPP current is low so that the duty ratio of input clocks are low; while when light intensity is high, as shown in Fig .5.6(b), the MPP current is high, so that the duty ratio of the input clocks are high. A transient measurements were also carried to verify the MPPT dynamic performance. As shown in Fig. 5.7, initially, the light intensity is low and the two PV outputs are 0.9V and 0.3V, respectively. Then the light intensity increases, and PV output voltage increases but reaches back to MPP voltage due to the MPPT control loop.

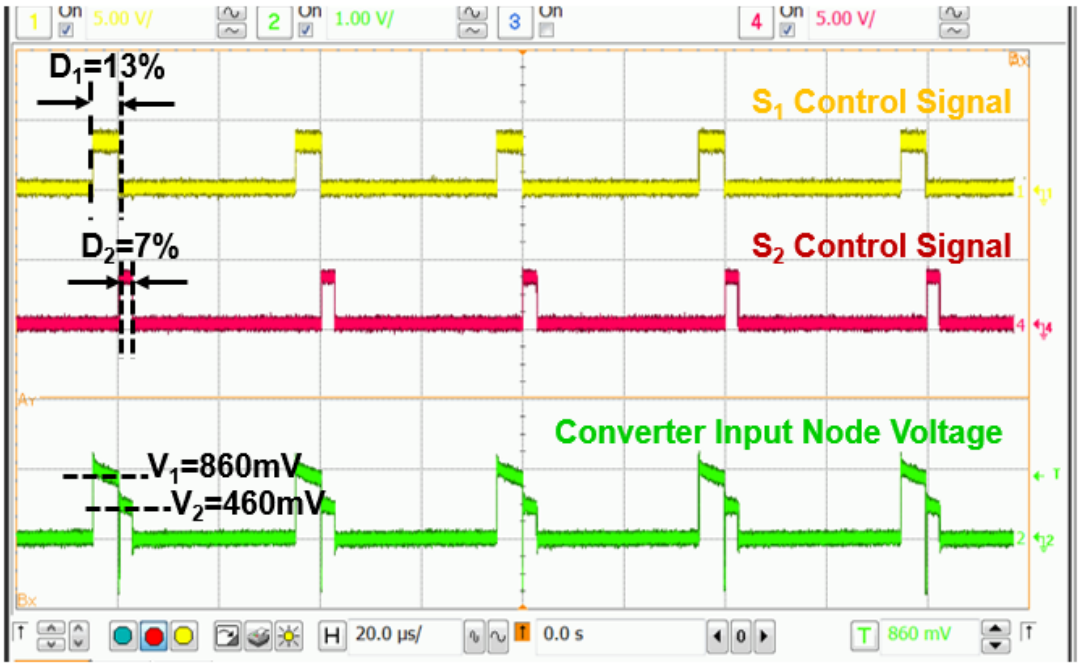

(a) Input Clock at Low Light Intensity

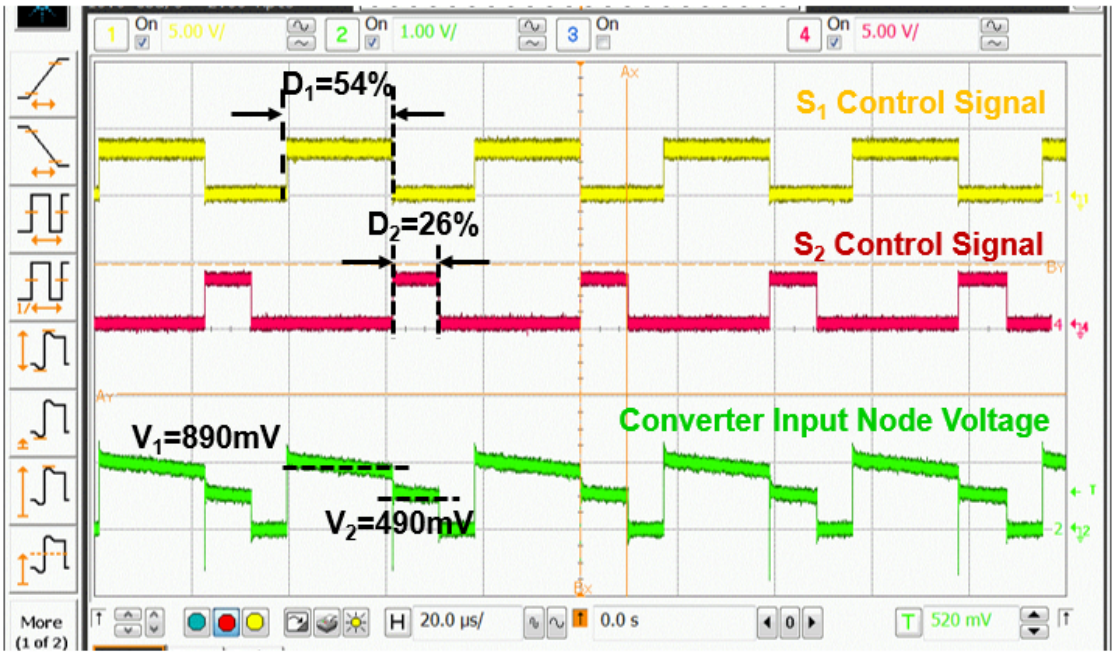

(b) Input Clock at High Light Intensity

Fig. 5.6 Input Clock Signals at Different Light Intensity

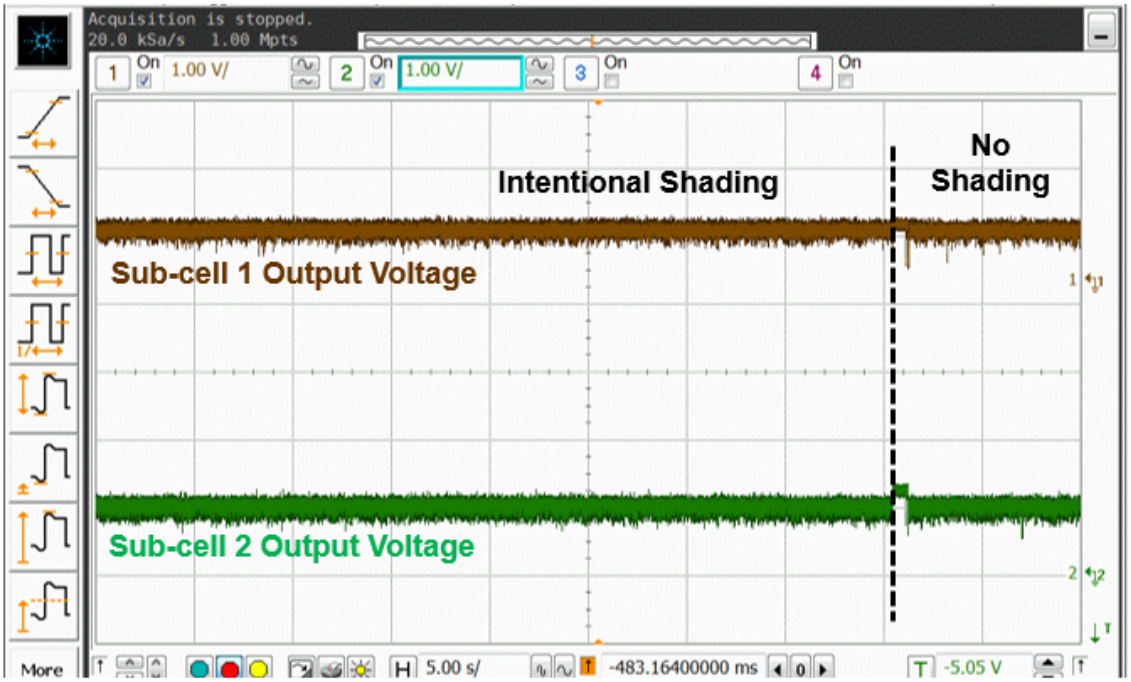

Fig. 5.7 MPPT Transient

Chapter 6

CONCLUSION AND FUTURE WORK

This thesis proposes a low cost, single-inductor, dual-input, CCM boost converter with MPPT for MJ-PV energy harvesting system. The input PV cells provide a few hundred milli-watt of power. CCM operation provides better efficiency than in DCM or PCCM. Inductor time-sharing provides a cost-effective solution for combining power from MJ-PV sub-cells. An inductor current regulation loop keep inductor current constant in both input condition and therefore reduces cross-regulation in CCM. A current-mirror based current sensor is used to sense instantaneous inductor current without causing any significant power loss. A modified hill climbing algorithm achieves MPPT for both sub-cells. A time-based power monitor senses PV power and the algorithm is based on PV current perturbation, which provides fast MPPT transient response. A dual-path output architecture provides a regulated output voltage of 2V. The boost converter works at around 1MHz and the input stages operates at around 100KHZ. The measured peak efficiency is around 85%.

Table 1 shows a comparison of the proposed system with previously published designs. Generally, DC-DC converters in DCM achieves higher efficiency at low input power, while that in CCM has better performance at higher input power. As can be seen, the proposed system processing higher PV power in CCM achieves higher peak efficiency than the inductor-sharing design processing lower PV input power in DCM. Although the peak efficiency of the proposed system is two percent lower than that of state-of-the-art single input boost converter, it has an advantage of less component count and much lower cost.

The future work includes the following:

1) Increase the number of inputs. This can be easily done with the same topology.

2) Recycling stored power in the secondary path using a buck converter. The buck converter delivers power from the storage unit (such as, battery or super capacitor) to one of the input of the multi-input boost converter.

3) To further increase the power efficiency, the inductor free-wheeling time must be minimized. An adaptive inductor current hysteresis window can be designed to dynamically minimize the inductor free-wheeling time.

Parameter	JSSC 2012 [14]	APEC 2011 [17]	ISSCC 2011 [19]	This Work
Energy Source	Photovoltaic, Thermoelectric and Vibration	PV panels	Single PV cell	MJ-PV Cell
Number of Inputs	3	multiple	1	2
Number of Inductors	1	1	1	1
Converter Operating Mode	DCM	PCCM	DCM	CCM
Maximum PV Output Power	2.5mW	170W	1.66mW	65mW
Peak Efficiency of power converters	83%	NA	87%	85%

Table 1. Comparison Table

REFERENCES

[1] C.H. Henry, “Limiting efficiencies of ideal single and multiple energy gap terrestrial solar cells”, J. Appl. Phys., 51(8), 1980

[2] R. R. King, A. Boca, W. Hong, D. Law, G. Kinsey, C. Fetzer, M. Haddad, K. Edmondson, H. Yoon, P. Pien, and N. Karem, “High-efficiency multi-junction photovoltaics for low-cost solar electricity,” in Proc. Ann. Meeting IEEE Lasers and Electro-Optics Society, Nov. 2008, pp. 2–3.

[3] R. R. King et al., “Solar cell generations over 40% efficiency,” Prog. Photovolt.: Res. Appl., vol. 20, pp. 801–815, 2012, doi: 10.1002/pip.1255.

[4] M. A. Green and A. Ho-Baillie, “Forty three per cent composite split-spectrum concentrator solar cell efficiency,” Prog. Photovoltaics: Res. Applicat., vol. 18, pp. 42–47, 2010.

[5] F. Dimroth, T. N. D. Tibbits, P. Beutel, C. Karcher, E. Oliva, G. Siefer, M. Schachtner, A. Wekkeli, M. Steiner, M. Wiesenfarth, A. W. Bett, R. Krause, E. Gerster, M. Piccin, N. Blanc, M. Muñoz Rico, C. Drazek, E. Guiot, J. Wasselin, C. Arena, T. Salvetat, A. Tauzin, T. Signamarcheix, T. Hannappel, “Development of high efficiency wafer bonded 4-junction solar cells for concentrator photovoltaic applications”, 40th IEEE Photovoltaic Specialist Conference, Denver, CO, 2014, pp. 840-843.

[6] B. R. Conley, H. Naseem, G. Sun, P. Sharps, and S.- Q. Yu, "High efficiency MJ solar cells and TPV using SiGeSn materials," in Photovoltaic Specialists Conference (PVSC), 2012 38th IEEE, 2012, pp. 001189-001192.

[7] T. Esram and P. L. Chapman, “Comparison of photovoltaic array maximum power point tracking techniques,” IEEE Trans. Energy Convers., vol. 22, no. 2, pp. 439–449, Jun. 2007.

[8] W. Xiao and W. G. Dunford, “A modified adaptive hill climbing MPPT method for photovoltaic power systems,” in Proc. 35th Annu. IEEE Power Electron. Spec. Conf., 2004, pp. 1957–1963.

[9]F. A. O. Aashoor and F. V. P. Robinson, “A Variable Step Size Perturb and Observe Algorithm for Photovoltaic Maximum Power Point Tracking,” Universities Power Engineering Conference (UPEC), 2012 47th International, pp. 1 - 6, 4 - 7 September 2012.

[10] B. N. Alajmi, K. H. Ahmed, S. J. Finney, and B. W. Williams, “Fuzzy logic-control approach of a modified hill-climbing method for maximum power point in microgrid standalone photovoltaic system,” IEEE Trans. Power Electron., vol. 26, no. 4, pp. 1022–1030, Apr. 2011.

[11] O. Wasynczuk, “Dynamic behavior of a class of photovoltaic power systems,” IEEE Trans. Power App. Syst., vol. 102, no. 9, pp. 3031–3037, Sep. 1983.

[12] H. Guan-Chyun, I. H. Hung, T. Cheng-Yuan, and W. Chi-Hao, “Photovoltaic power-increment-aided incremental-conductance MPPT with two-phased tracking,” IEEE Trans. Power Electron., vol. 28, no. 6, pp. 2895–2911, Jun. 2013.

[13] P. Midya, P. T. Krein, R. J. Turnbull, R. Reppa, and J. Kimball, “Dynamic maximum power point tracker for photovoltaic applications,” in Proc. 27th Annu. IEEE Power Electron. Spec. Conf., 1996, pp. 1710–1716.

[14] S. Bandyopadhyay, A.P. Chandrakasan, "Platform architecture for solar, thermal and vibration energy combining with MPPT and single inductor," IEEE Journal of Solid-State Circuits,, vol. 47, no. 9, pp. 238-239, June 2012.

[15] M. Alam, F. Khan, and A. Imtiaz, “Optimization of sub-cell interconnection for multi-junction solar cells using switching power converters,” IEEE Trans. Sustain. Energy, vol. 4, no. 2, pp. 340–349, Apr. 2013.

[16] J. Abu Qahouq and Y. Jiang, "Distributed photovoltaic solar system architecture with single-power inductor single-power converter and single-sensor single maximum power point tracking controller," IET Power Electronics, vol. 7, no. 10, pp. 2600-2609, Oct. 2014.

[17] S. Poshtkouhi and O. Trescases, “Multi-input single-inductor dc–dc converter for MPPT in parallel-connected photovoltaic applications,” in Proc. 26th Annu. IEEE Appl. Power Electron. Conf. Expo., 2011, pp. 41–47

[18] S. Uprety and H. Lee, “A 43V 400mW-to-21W global-search-based photovoltaic energy harvester with 350 μs transient time, 99.9 % MPPT efficiency, and 94 % power efficiency,” in Dig. Tech. Papers IEEE Int. Solid-State Circuits Conf. (ISSCC), 2014, pp. 404–405.

[19] Y. Qiu, C.V. Liempd, B.O. Veld, P.G. Blanken, and C.V. Hoof, "53W-to- 10mW Input Power Range Inductive Boost Converter for Indoor Photovoltaic Energy Harvesting with Integrated Maximum Power Point Tracking Algorithm," in Proc. IEEE International Solid-State Circuits Conference Digest of Technical Papers, pp. 118-119, Feb. 2011.